



2 Computer simulation of the role of groundwater seepage in forming 3 Martian valley networks

4 Wei Luo¹ and Alan D. Howard²

5 Received 7 August 2007; revised 29 January 2008; accepted 20 February 2008; published XX Month 2008.

6 [1] The role of groundwater in forming Martian valley networks is simulated in a
7 computer model as seepage erosion by contributing to surface runoff and as seepage
8 weathering by causing accelerated weathering of bedrock, which makes its subsequent
9 erosion and removal easier. Simulation results show that seepage erosion cannot mobilize
10 large grain size sediment and is marginally effective at generating integrated valley
11 networks with realistic rates of aquifer recharge. On the other hand, seepage weathering
12 may play a major role in forming Martian valley networks. Seepage weathering combined
13 with fluvial runoff creates stubby deep canyons with abrupt headwalls that are similar
14 in morphology to terrestrial and Martian valley systems attributed to erosion by
15 groundwater. Depending on the relative contribution of groundwater weathering to surface
16 runoff erosion, a continuum of valley network morphology can be generated. Eolian
17 modification masks the original differences in fluvial landforms, making different
18 scenarios visually more similar. Martian valley networks may have developed through a
19 range of combinations of runoff erosion and seepage weathering, which can complicate
20 the interpretation of the processes based on final landform morphology. Unequivocal
21 identification of seepage involvement of valley incision on Mars may not be possible
22 without knowledge of subsurface properties (hydraulic conductivity, layering, degree of
23 cementation, etc.) and the grain sizes of sediment transported through the valley systems.

24 **Citation:** Luo, W., and A. D. Howard (2008), Computer simulation of the role of groundwater seepage in forming Martian valley
25 networks, *J. Geophys. Res.*, 113, XXXXXX, doi:10.1029/2007JE002981.

27 1. Introduction

28 [2] The processes forming Martian valley networks
29 (VNs) have important implications for the hydrologic cycle
30 and associated potential for life on Mars. Theater-headed
31 valleys on Mars, also characterized by short stubby tributaries,
32 near constant valley width, U-shaped cross section, low
33 drainage density, and irregular longitudinal profile, similar
34 to those observed in Colorado plateau [Laity and Malin,
35 1985], have often been attributed to erosion by emerging
36 groundwater (i.e., seepage erosion or groundwater sapping)
37 rather than by surface runoff [Sharp and Malin, 1975; Pieri,
38 1980b; Carr, 1996]. This mechanism of valley formation
39 would not necessarily require conditions much warmer than
40 the current cold climate. However, some more recent studies
41 using higher-resolution data have revealed the importance
42 of fluvial surface runoff and by inference at least some
43 precipitation on early Mars [Craddock and Howard, 2002;
44 Mangold et al., 2004; Mangold and Ansan, 2006; Howard,
45 2007]. In addition, a number of studies have cast some
46 uncertainties on groundwater sapping as the sole mechanism

for forming either terrestrial or Martian valleys with 47
“typical” sapping characteristics [Irwin et al., 2006; Lamb 48
et al., 2006]. These new developments call for careful 49
reevaluation of the evidence that supports groundwater 50
sapping origin of VNs. Computer simulation of landform 51
development on Mars offers a valuable tool to explore the 52
relative importance of groundwater versus surface water in 53
forming Martian VNs. Previous computer modeling of 54
groundwater sapping mostly focuses on terrestrial context 55
[Howard, 1988; Luo et al., 1997]. Howard [2007] recently 56
used computer simulation to better understand the interplay 57
between impact cratering and fluvial erosional processes in 58
forming Martian highland landscapes. This paper is a 59
natural extension of that study focusing on the interplay 60
between surface fluvial processes and groundwater seepage 61
processes, which has not been reported. 62

2. Definition of Terms 63

[3] In order to avoid confusion, we adopted the termi- 64
nology proposed by Dunne [1990] and also followed by 65
Lamb et al. [2006]. Weathering processes that are facilitated 66
by emerging groundwater or seepage (e.g., salt precipita- 67
tion, chemical dissolution or frost growth) are collectively 68
referred to as seepage weathering. The removal of mass 69
from a seepage face by exfiltrating flow is termed seepage 70
erosion. In unconsolidated sediments, seepage erosion can 71
occur in the absence of seepage weathering if the discharge 72

¹Department of Geography, Northern Illinois University, DeKalb, Illinois, USA.

²Department of Environmental Sciences, University of Virginia, Charlottesville, Virginia, USA.

73 of seepage water is sufficient to detach and mobilize the
 74 sediment. However, in rock, seepage weathering is needed
 75 to render the rock cohesionless before fluvial erosion can
 76 occur, either by seepage erosion or runoff. Sapping
 77 describes processes that undercut or undermine a scarp
 78 leading to an overhang. A variety of processes cause
 79 sapping (e.g., cut bank erosion by a meandering river, wave
 80 erosion of a sea cliff, seepage erosion at the base of a scarp
 81 or headwall, plunge pool erosion at the base of a waterfall).
 82 The term groundwater sapping then refers to sapping
 83 induced by seepage erosion.

84 3. Model and Its Parameterization

85 [4] The computer model has been developed by Howard
 86 [Howard, 1994, 1997, 2007; Forsberg-Taylor et al., 2004].
 87 It can simulate impact cratering, lava flows, eolian modifica-
 88 tion, and drainage basin processes, including physical or
 89 chemical weathering of rocks to form transportable collu-
 90 vium, mass wasting by nonlinear creep, fluvial detachment,
 91 and fluvial transport and deposition, and groundwater
 92 sapping [Howard, 1994, 1997, 2007; Forsberg-Taylor et
 93 al., 2004]. The model incorporates mass wasting, which at
 94 the scale of the present simulations primarily results in
 95 valley side slopes being at approximately the angle of
 96 repose for cohesionless materials. For details of how the
 97 fluvial erosion and impact cratering processes are modeled,
 98 please refer to Howard [1994, 2007]. Here we briefly
 99 outline the model and its parameterization, with more
 100 details on groundwater modeling.

101 3.1. Groundwater Flow Governing Equation

102 [5] Valley erosion on Earth as a result of groundwater
 103 seepage occurs in two very distinct settings, seepage erosion
 104 in unconsolidated sediments and seepage weathering of
 105 coherent rocks. Our simulation scenarios target these two
 106 terrestrial end-member cases in order to provide some
 107 insights into the Martian processes.

108 [6] The source of the groundwater can be as a result of
 109 nearby surface recharge, contributions from distant recharge
 110 sources as in artesian groundwater seeps, or by hydrother-
 111 mally induced groundwater circulation [Gulick and Baker,
 112 1989; Gulick, 1998]. We assume, however, water input in
 113 the model is from precipitation, which can either flow as
 114 surface runoff or infiltrate and reemerge in seeps and
 115 springs to feed surface drainage. We also assume that before
 116 the end of heavy bombardment, Martian landscape would
 117 be dominated by impact cratering. We focus on simulating
 118 the modification of the cratered terrain by surface runoff
 119 water and emerging groundwater after heavy bombardment.
 120 The model also assumes uniform bedrock material strength
 121 and does not simulate effects of layers of different strength.

122 [7] Groundwater flow has been included in the drainage
 123 basin model represented as unconfined, steady state DuPuit
 124 flow (vertical flow components much smaller than horizon-
 125 tal components). The governing equation is

$$\frac{\partial}{\partial x} \left(\left[\int_{-\infty}^{h_w} K(z) dz \right] \frac{\partial h_w}{\partial x} \right) + \frac{\partial}{\partial y} \left(\left[\int_{-\infty}^{h_w} K(z) dz \right] \frac{\partial h_w}{\partial y} \right) + I_{xy} = 0, \quad (1)$$

where x and y are the horizontal axes, K is an horizontally
 isotropic but possibly a really varying hydraulic conductiv-
 ity that varies with elevation z , h_w is the water table
 elevation, and I_{xy} is recharge (due to infiltrating precipita-
 tion or hydrothermal upwelling). Hydraulic conductivity is
 assumed to decrease as a negative exponential function with
 depth from a value of K_0 at the ground surface at $z = z_s$,

$$K(z) = K_0 e^{-\beta(z_s - z)}, \quad (2)$$

where β governs how rapidly hydraulic conductivity decays
 with depth.

[8] Clifford and Parker [2001], following Manning and
 Ingebritsen [1999], suggest crustal permeability declines in
 proportion to the logarithm of depth. However, since this
 functional form does not give a finite surface permeability
 (or hydraulic conductivity), we assume in equation (2) that
 hydraulic conductivity declines as a negative exponential of
 depth in a functional relationship similar to that proposed by
 Clifford and Parker [2001] for porosity. The model for
 porosity decrease proposed by Clifford and Parker [2001]
 suggests that porosity diminishes by a factor two in the first
 two kilometers below the surface. The scaled permeability
 relationship by Clifford and Parker [2001] suggests an even
 more rapid decay rate with depth, decreasing by about 1
 order of magnitude between 1 and 2 km below the surface.
 Using hydrogeologic, thermal, seismic, and magmatic mod-
 eling constraints, Saar and Manga [2004] also found that
 for shallower depths (typically $z \leq 0.8$ km and up to $z \leq$
 2 km) an exponential relationship for permeability “fits data
 better (at least for the Cascades and seemingly for conti-
 nental crust in general).”

[9] Thus, equation (1) can be expressed in the more
 typical form of the DuPuit-Forsheimer equation by express-
 ing the integral as the product of the surface hydraulic
 conductivity and an effective aquifer depth, h_e

$$\frac{\partial}{\partial x} \left(K_0 h_e \frac{\partial h_w}{\partial x} \right) + \frac{\partial}{\partial y} \left(K_0 h_e \frac{\partial h_w}{\partial y} \right) + I_{xy} = 0, \quad (3)$$

where, substituting equation (2), h_e is given by

$$h_e = \frac{e^{-\beta(z_s - h_w)}}{\beta}. \quad (4)$$

This form of the equation is used in model calculations.
 (Note if we define an effective transmissivity T_e as $T_e = K_0$
 h_e , equation (3) takes a more standard form). The model
 assumes a steady state groundwater flow. The water table
 configuration is found by an iterative solution to the finite
 difference approximation of the equation, starting from a
 level water table at the elevation of the lowest topographic
 point. Initially only this lowest point is fixed head. During
 the iterative solution any calculated water table elevation
 that is higher than the surface elevation is converted to fixed
 head, and the solution continues until convergence to a
 stable water table. Figure 1d shows an example of a final
 water table surface. During each iteration, equation (4) must
 be solved for the value of h_e and the head gradients must be
 determined for substitution in equation (3). At fixed head
 locations equation (3) is solved for I_{xy} ; negative values

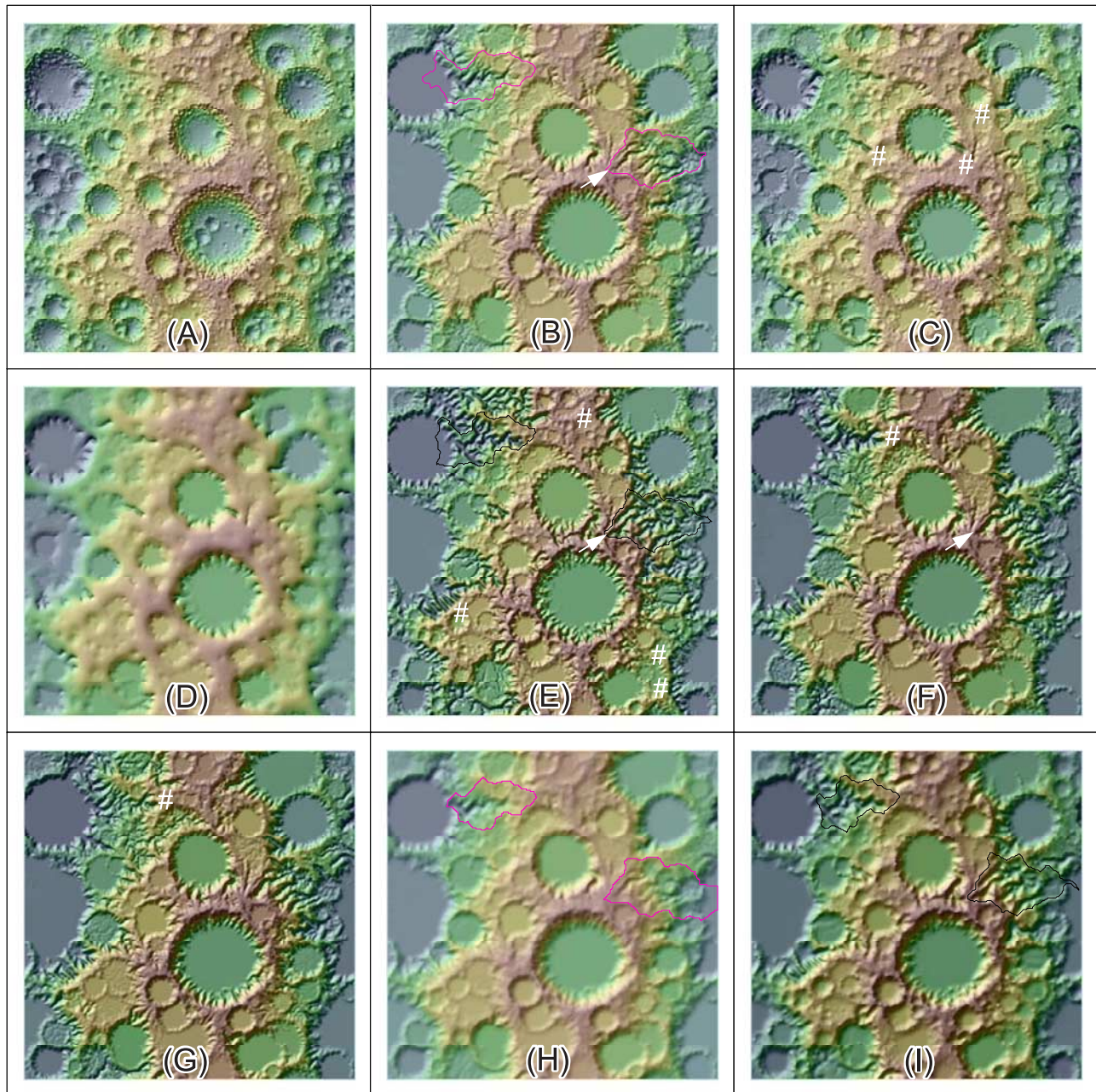


Figure 1. Shaded relief maps of simulation results. Color ramp from blue to brown indicates elevation or water table from low to high. (a) Initial conditions of simulation (a cratered terrain). (b) Erosion solely by surface water fluvial erosion (no groundwater involvement). Pink lines outline two basins whose hypsometric curves are shown in Figure 4. (c) Groundwater seepage erosion (all precipitation infiltrates into ground and seeps out as groundwater discharge that contributes to surface flow) on unconsolidated sediments (grain size diameter = 0.0002 m, recharge rate = 1 m/a, $\beta = 0.00347$) (d) Groundwater table for Figure 1c. (e) Same as for Figure 1c except $\beta = 0.00693$. Black lines outline two basins whose hypsometric curves are shown in Figure 4. (f) Seepage weathering on bedrock with negligible groundwater contribution to surface flow, but groundwater seepage causes accelerated weathering of bed rock ($W_s = 0.002$). Fluvial erosion uses same conditions as in Figure 1b. (g) Same as for Figure 1e except $W_s = 0.001$. (h) Eolian modification of Figure 1b. Pink lines outline two basins whose hypsometric curves are shown in Figure 4. (i) Eolian modification of Figure 1e. Black lines outline two basins whose hypsometric curves are shown in Figure 4.

180 imply water discharged to the surface. This discharge is
181 routed downstream, adding to surface flow from runoff.

182 3.2. Seepage Erosion in Unconsolidated Sediment

183 [10] Direct entrainment and transport of sediment by
184 seepage occurs in the classic cases of beach erosion during
185 falling tides [e.g., *Higgins*, 1984; *Otvos*, 1999] and on
186 noncohesive river banks during falling river stages [e.g.,
187 *Budhu and Gobin*, 1995]. Seepage erosion has been impli-
188 cated in the erosion and maintenance of channel heads [e.g.,
189 *Dunne*, 1980, 1990; *Higgins*, 1982, 1984; *Schumm and*
190 *Phillips*, 1986; *Montgomery and Dietrich*, 1989; *Coelho*
191 *Netto and Fernandes*, 1990; *Teixeira De Oliveira*, 1990;
192 *Gehrels and Van De Plassche*, 1992; *Uchupi and Oldale*,
193 1994; *Schumm et al.*, 1995; *Nash*, 1996; *Gabbard et al.*,
194 1998; *Spence and Sauchyn*, 1999; *Gutierrez et al.*, 2003;
195 *Froede and Williams*, 2004]. Theory and laboratory experi-
196 ments in fine-grained cohesionless sediment demonstrate
197 the ability of seepage flow to excavate valleys [*Kochel et*
198 *al.*, 1985, 1988; *Howard*, 1988; *Howard and McLane*,
199 1988; *Gomez and Mullen*, 1992; *Lobkovsky et al.*, 2004;
200 *Shorghofer et al.*, 2004; *Ni and Capart*, 2006]. Emergent
201 groundwater fluxes sufficient to erode and transport sedi-
202 ment depend upon source deposit grain sizes small enough
203 to be transported (generally finer than gravel) and large
204 enough to support sufficient groundwater flow (generally
205 sand size or larger). Groundwater contributions to valley
206 erosion can also occur in fine-grained cohesive sediment
207 through hydraulic erosion and slaking by flow through
208 discrete subsurface openings (“piping” [e.g., *Jones*, 1971,
209 1987; *Nwankwor et al.*, 1998; *Tomlinson and Vaid*, 2000;
210 *Onda*, 2002]).

211 [11] We consider only erosion of cohesionless sediment
212 in the direct erosion and transport and assume subsurface
213 deposits with a surface hydraulic conductivity, K_0 , of
214 about $0.31 \times 10^{-5} \text{ m s}^{-1}$ (equivalent to silty to clean
215 sands [*Freeze and Cherry*, 1979]) and a generous recharge
216 (1 m/a, where a is years). This combination of parameters
217 allows sufficient emergent groundwater flux to be able to
218 erode sand-sized particles. As discussed by *Howard and*
219 *McLane* [1988], the erosion of cohesionless sediment by
220 emergent groundwater is largely regulated by the ability of
221 the fluvial flows to remove sediment from the stream head
222 and direct sediment destabilization by seepage is restricted
223 to a very narrow zone. As a result, in these simulations we
224 do not include any special process within seepage chan-
225 nels over and above normal fluvial transport in response to
226 the total discharge of water resulting from groundwater
227 discharge.

228 [12] All rainfall on unsaturated uplands is assumed to
229 infiltrate and to eventually reemerge in seepage locations
230 and contribute to total runoff. All rainfall on saturated
231 locations with effluent groundwater, however, is assumed
232 to contribute to total runoff (in addition to the groundwater
233 seepage contribution). In these simulations the bed material
234 is assumed to be sand with a grain size of 0.2 mm. Two
235 simulations are reported here, one with the hydraulic
236 conductivity decay constant, $\beta = 0.00347$ (hydraulic con-
237 ductivity decreases to half its surface value 200 m below the
238 surface) and $\beta = 0.00693$ (half value at 100 m depth).

239 [13] For the erosion of unconsolidated sediment, we
240 assume that no weathering occurs to the sediment prior to

erosion, which, in the simulation model, is equivalent to an 241
infinite thickness of regolith. 242

3.3. Seepage Erosion by Bedrock Weathering 243

[14] The second case of enhanced weathering of rock at 244
zones of emergent seepage targets development of canyons 245
in permeable bedrock through weakening and undermining 246
of the rock in canyon headwalls, as proposed for some 247
canyons developed in the Navajo Sandstone Formation of 248
the southwestern United States [e.g., *Laity*, 1983; *Laity and* 249
Malin, 1985; *Howard and Kochel*, 1988; *Howard and* 250
Selby, 1994]. Although *Laity and Malin* [1985] suggest 251
that emergent seepage may directly erode the mass-wasted 252
wall rock, *Howard and Kochel* [1988] and *Lamb et al.* 253
[2006] argue that surface flows from seepage are insuffi- 254
cient to remove even sand-sized debris and that direct 255
surface runoff is responsible for removal of sapping debris 256
(although additional size reduction of mass wasting debris 257
may occur because of weathering by seepage). Accord- 258
ingly, we assume that the role of emergent groundwater is 259
primarily to provide enhanced weathering to enhance 260
erosion of bedrock by runoff. We target our simulations 261
to canyon erosion in materials with properties similar to the 262
Navajo Sandstone. Hydraulic conductivity of the Navajo 263
Sandstone varies widely because of differences in porosity, 264
cementing, and fracture density. Estimated values range 265
over several orders of magnitude, from about 1×10^{-7} to 266
 1×10^{-4} m/s, with typical averages about 2×10^{-6} m/s 267
[e.g., *Brown and Eychaner*, 1988; *Heilweil et al.*, 2000, 268
2007; *Thomas*, 2002]. In the Navajo Sandstone, seepage 269
often occurs from minor exposed aquicludes or above the 270
shaly layers at the contact between the Navajo and the 271
underlying Kayenta Formation. To compensate for the lack 272
of aquicludes in the model, we assume a fairly small 273
hydraulic conductivity of 1.2×10^{-7} m/s to give high 274
groundwater levels for reasonable recharge rates. Recharge 275
rates into the Navajo Sandstone typically range from 0.005 276
to 0.05 m/a, averaging about 0.02 m/a [*Zhu*, 2000; *Heilweil* 277
et al., 2007]. These recharge rates correspond to about 10% 278
of yearly precipitation. Again, to produce relatively 279
high groundwater levels in our simulations, we assume a 280
recharge rate near the high end of the observed spectrum, 281
0.04 m/a. 282

[15] The mechanisms by which seepage reduces rock 283
strength are uncertain and not quantified. Crystal growth, 284
cement dissolution, biotic activity on the seepage face 285
(typically vegetated), and freeze-thaw are possible processes 286
[*Laity*, 1983; *Howard and Kochel*, 1988]. Despite the 287
process uncertainty, seepage faces nearly universally occur 288
at the deepest part of valley headwall alcoves, indicating a 289
positive relationship between bedrock erosion and occur- 290
rence of seepage. Scarp retreat through seepage weathering 291
was simulated by *Howard* [1995] with the assumption that 292
the rate of scarp retreat was proportional to a power law 293
relationship to seepage specific discharge. These simula- 294
tions demonstrated that scarp retreat in proportion to seep- 295
age specific discharge is sufficient to create canyons with 296
nearly constant width, rounded headwalls, and stubby 297
branching of the type observed in canyons in the Navajo 298
Sandstone characterized by seepage alcoves. In the present 299
simulations we assume that the bedrock weathering rate, 300
 \dot{z}_b (m/a), is enhanced in proportion to the seepage flux 301

302 divergence, I_{xy} (m/a), which quantifies the seepage specific
303 discharge to the surface

$$\dot{z}_b = W_0 e^{-\omega H} + W_s I_{xy}, \quad (5)$$

305 where H is regolith thickness (m), W_0 is the background
306 weathering rate (m/a), and W_s is the rate of weathering
307 induced by groundwater seepage. In the absence of
308 applicable theory or quantitative measurements, we have
309 adopted a simple linear relationship as test of the efficacy of
310 seepage weathering to affect the course of fluvial erosion.
311 We assume $\omega = 0.03 \text{ m}^{-1}$, $W_0 = 0.0001 \text{ m/a}$, and $W_s = 0.002$
312 for the nominal case. The small value of the background
313 weathering rate, W_0 , means that weathering will be very
314 slow except in locations with emergent seepage. Erosion by
315 surface discharge is parameterized as a function of direct
316 runoff using the same process formulation as the case of
317 pure runoff erosion (see below). For this case seepage flows
318 make a negligible contribution to total surface flows.

319 3.4. Runoff Erosion Model

320 [16] The landscape model, used in the simulations
321 reported here, is essentially the DELIM model as reported
322 by Howard [1994, 1997, 2007] and Forsberg-Taylor *et al.*
323 [2004] with components modeling physical or chemical
324 weathering of rocks to form transportable colluvium, mass
325 wasting by nonlinear creep, fluvial detachment, and fluvial
326 transport and deposition. Parameters used for these simu-
327 lations are based upon terrestrial values in semiarid or arid
328 landscapes except for correcting for the difference in gravity
329 between Mars and Earth. We briefly outline the model
330 below, and additional background and model details can
331 be found by Howard [1994, 1997, 2007].

332 [17] It is assumed that the materials below the surface
333 (lava, sediments, ejecta, etc., collectively termed “bed-
334 rock”) may be indurated, but can be weathered at a finite
335 rate by physical or chemical processes to form colluvium.
336 The rate of bedrock weathering is given by equation (5)
337 with the seepage weathering term, W_s , set to zero. Note that
338 \dot{z}_b is the rate of lowering of the colluvial bedrock contact,
339 and when weathering is isovolumetric, as is assumed here, it
340 does not change the land surface elevation.

341 [18] The potential rate of erosion by mass wasting, \dot{z}_m ,
342 is proportional to the spatial divergence of colluvial mass
343 flux, q_m

$$\dot{z}_m = -\nabla \cdot q_m. \quad (6)$$

345 Colluvial flux is given by a nonlinear relationship

$$q_m = \left[K_s |S| + K_t \left(\frac{1}{1 - \{|S|/S_t\}^a} - 1 \right) \right] s, \quad (7)$$

347 where $|S|$ is the absolute value of local slope, s is the unit
348 vector in the downslope direction, a is an exponent with an
349 assumed value of 3.0, S_t is a threshold gradient at which the
350 rate of mass wasting becomes infinite (i.e., landsliding), and
351 K_s is creep diffusivity. K_t takes a value (0.5) that provides
352 for a smooth but rapid approach to threshold slopes for
353 rapid rates of erosion. Erosion of bare bedrock slopes
354 (exposed when rates of erosion are greater than the

maximum weathering rate given by equation (5)) follows
equation (7), but with K_s set to zero and a steeper critical
gradient, S_c , of 2.7. Erosion of bedrock slopes involves a
wide variety of processes and resultant forms [e.g., Howard
and Selby, 1994]), and the assumed critical gradient (about
70°) is chosen to represent bedrock slopes in rapidly
incising canyons.

[19] Because of the large cell size in the simulations
discussed below (400 m) mass transport by linear creep
(K_s in equation (7)) and the shape of small slopes is not well
characterized. Longer slopes in rapidly eroding locations
(e.g., on crater rims), however, tend to be close to the
threshold gradient (0.8).

[20] In the present modeling potential erosion by fluvial
detachment, \dot{z}_f in bedrock and regolith-floored channels and
on steep slopes where the flow is carrying less than a
capacity load is assumed to be proportional to the shear
stress, τ , exerted by flowing water

$$\dot{z}_f = -K_f (\tau - \tau_c), \quad (8)$$

where K_f is a parameter with units $\text{m}^2 \text{ a kg}^{-1}$. The critical
shear stress, τ_c , is assumed to be zero in the present
simulations. Assuming that the reference shear stress is that
which corresponds to the mean annual flood, the value of K_f
that we assume ($0.0001 \text{ m}^2 \text{ a kg}^{-1}$) corresponds to
terrestrial rates of erosion in moderately strong sedimentary
rocks. For the case of direct seepage erosion we assume a
weaker substrate with $K_f = 0.01 \text{ m}^2 \text{ a kg}^{-1}$.

[21] Flow of water is assumed to be channelized and
originating from runoff. Shear stress can be related to
channel gradient and drainage area using equations of
hydraulic geometry and steady, uniform flow as discussed
by Howard [1994, 2007]

$$\tau = \rho_f g R S, \quad (9)$$

$$V = K_n g^{1/2} R^{2/3} S^{1/2} / N, \quad (10)$$

$$Q = R W V, \quad (11)$$

$$Q = P A^e, \quad (12)$$

$$W = K_w Q^b, \quad (13)$$

where R is hydraulic radius, S is channel gradient, V is mean
velocity, N is Manning’s resistance coefficient, P is a
specific runoff yield (depth per unit area per unit time), Q is
an effective discharge, W is channel width, A is drainage
area, and K_n , K_p , K_a , K_w are coefficients. Channel width, as
parameterized in equation (13), is generally much less than
the size of an individual grid cell, and following Howard
[1994], each grid cell is assumed to host a single channel
that carries the total discharge through that cell. The
coefficients and exponents in equations (9)–(13) are
assumed temporally and spatially invariant. The following
parameter values are assumed: $N = 0.03$, $K_n = 0.3$ (for

metric units); $P = 3.5 \times 10^{-7}$ m/s, $e = 1.0$, $b = 0.5$, and $K_w = 5.0 \text{ s}^{0.5} \text{ m}^{-0.5}$.

[22] Regolith is assumed to be more erodible than the bedrock by a factor $M = 10.0$, which is assumed to influence the bed erodibility and the threshold of erosion; thus, the potential rate of fluvial erosion of channels flowing on regolith, \dot{z}_r , is calculated from equation (8) by multiplying K_f by M and dividing τ_c by M .

[23] When the flux of sediment transported as bed and suspended load reaches or exceeds the transporting capacity of the flow (an alluvial channel as opposed to a bedrock channel), the rate of erosion or deposition, \dot{z}_f , is proportional to the spatial divergence of transport flux q_s (volume per unit time per unit width)

$$\dot{z}_f = -\nabla \cdot q_s \quad (14)$$

[24] Sediment transport flux is estimated using a bed load transport formula that expressed as the relationship between a dimensionless transport rate, Φ , and a dimensionless shear stress, τ^*

$$\Phi = K_e \{ \tau^* - \tau_c^* \}^p, \quad (15)$$

where

$$\Phi = \frac{q_{sb}(1 - \mu)}{g^{1/2} d^{3/2} (S_s - 1)^{1/2}} \quad (16a)$$

and

$$\tau^* = \frac{\tau}{\rho_f g (S_s - 1) d}. \quad (16b)$$

[25] In these equations τ_c^* is the value of τ^* at the threshold of motion, q_{sb} is bed sediment transport rate in bulk volume of sediment per unit time per unit channel width, S_s is the specific gravity of the sediment, g is gravitational acceleration, ρ_f is the fluid density, d is the sediment grain size, and μ is alluvium porosity. We assume a sand bed with $d = 0.0002$ m, $K_e = 40.0$, and $p = 1.5$. For all simulations $\tau_c^* = 0.05$, and $S_s = 2.65$ and $\mu = 0.5$. The shear stress is estimated from equations (9)–(13), with the dominant discharge for sediment transport assumed to be 0.6 of the mean annual flood, flowing 3% of the year. However, for the seepage erosion simulations (section 3.2) we assume that the dominant discharge is that from groundwater discharge and that the flow is constant (100% of the year). Rivers vary from those transporting dominantly suspended load to those carrying primarily bed load [e.g., Schumm, 1977]. In the absence of information for Martian channels, bed sediment load is assumed to constitute 20% of sediment eroded from slopes.

3.5. Eolian Modification Model

[26] Eolian modification is based upon an exposure index, I_e , which is based upon a weighted sum of the gradients, S_i , between the local elevation, E , and that of a surrounding location, E_i

$$S_i = [(E_i - E) / \Delta x_i], \quad (17)$$

where Δx_i is the distance to the nearby point [Forsberg-Taylor et al., 2004]. The exposure index, I_{ek} , for points lying along a transect, k , extending from the given location is given by

$$I_{ek} = \sum_{i=1}^n S_i e^{-\eta \Delta x_i} / \sum_{i=1}^n e^{-\eta \Delta x_i}, \quad (18)$$

where the parameter η governs the relative importance of nearby versus distant points in determining the exposure [Forsberg-Taylor et al., 2004]. Points that are not visible from the location (lying behind a closer high point) are not included. For computational efficiency exposure indices are calculated only along the eight cardinal and diagonal directions from a given point and the net exposure index, I_e , is the average of the eight I_{ek} . The rate of eolian erosion or deposition, $\partial z / \partial t|_e$ is a function of the exposure index. We used the same functional dependence of eolian erosion on exposure index as illustrated in Figure 3 of Forsberg-Taylor et al. [2004]. Eolian erosion and deposition need not occur simultaneously. Deposition can occur from a nearly still atmosphere, whenever dust loading occurs from dust storms, crater impacts, or volcanic eruptions. Erosion occurs on exposed areas during strong wind events. Further description of the eolian model is presented by Forsberg-Taylor et al. [2004].

4. Results

[27] For easy comparison and better understanding of the processes, we first present the simulations starting with the same initial cratered terrain as shown in Figure 1a and we will then briefly discuss the result with a different initial condition. The grid size is 256 by 256 with each cell having a dimension of 400 by 400 m. The whole simulation domain has dimension of about 102 by 102 km. All scenarios were run for 2500 iterations, which roughly correspond to a minimum of 2.5 million years on the basis of terrestrial process rate scaling in arid to semiarid climates. We now describe the result of each scenario in more detail.

[28] The simulations have been conducted to examine whether groundwater involvement in fluvial erosion imparts distinctive morphology to the resulting landscape. It has long been postulated that the signature morphology of groundwater erosional processes are sparse, weakly branched, box canyons with abrupt, theater-shaped headwalls [e.g., Higgins, 1982, 1984; Laity and Malin, 1985; Howard and Kochel, 1988]. Our simulations of groundwater involvement in erosion of cratered landscapes tend to confirm this signature morphology.

4.1. Surface Discharge Solely From Runoff

[29] Erosion dominated by runoff erosion produces landscapes with fairly uniform intensity of dissection on upland slopes, strongly dendritic valley networks, and narrow valleys that gradually shallow headward (Figure 1b), typical of fluvially eroded landscapes. Additional examples of runoff erosion of cratered surfaces are presented by Howard [2007] for a variety of hydrologic scenarios and for some simulations with concomitant impact cratering. The fluvially dominated simulation in Figure 1b assumes a dominantly weathering-limited landscape with a relatively

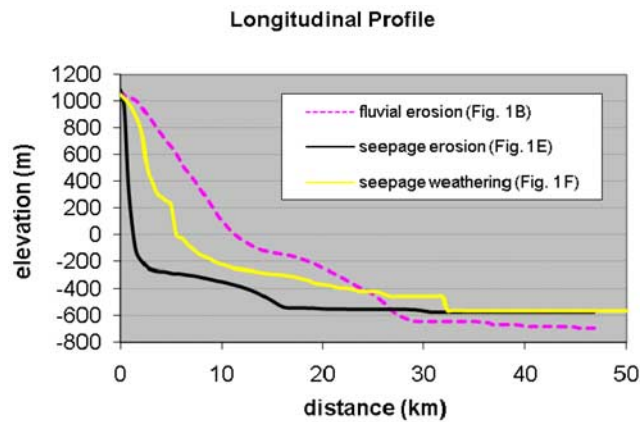


Figure 2. Longitudinal profiles of the valley networks pointed by white arrow in Figures 1b, 1e, and 1f.

516 slow rock weathering rate (0.0001 m/a) and it serves as a
517 process comparison to the two scenarios of seepage-related
518 erosion. The longitudinal profile of a valley started at the
519 location pointed by the white arrow is shown in Figure 2,
520 which is a concave upward profile typical of fluvial erosion.

521 4.2. Seepage Erosion in Unconsolidated Sediments

522 [30] Direct erosion by groundwater seepage is possible in
523 fine-grained cohesionless sediment as, for example, the
524 small valleys excavated on beaches during falling tides.
525 Under this scenario, we assume that impact cratering at the
526 end of heavy bombardment has created unconsolidated,
527 cohesionless sediments (megaregolith) covering at least
528 some areas of Mars, which can be subject to seepage
529 groundwater erosion.

530 4.2.1. Case 1: Deep Effective Aquifer Depth ($h_e = 200$ m, $\beta = 0.00347$)

532 [31] Our simulations assumed a subsurface material char-
533 acterized by a hydraulic conductivity typical of sand ($0.31 \times$
534 10^{-5} m/s) and a recharge of 1.0 m/a. The simulation shown
535 in Figure 1c assumes that hydraulic conductivity decreases
536 as a negative exponential of depth beneath the surface
537 (equation (2)), decreasing to half its surface value at a
538 depth of 200 m. With this simulation, about 12% of the
539 land surface initially experienced groundwater seepage to
540 the surface, increasing to about 18% by the end of the
541 simulation. Figure 1d shows the configuration of the water
542 table at the close of the simulation. During the simulation,
543 short stubby valleys formed along the lower interior walls of
544 large impact craters (e.g., the large crater in the center of
545 Figure 1c) and a few unbranched, short, flat-floored can-
546 yons eroded from low areas toward major groundwater
547 divides (e.g., near “the number sign” in Figure 1c). Even
548 with the high recharge rate and high hydraulic conductivity,
549 fluvial erosion had essentially ceased by the end of the
550 simulation, because the low-gradient fluvial valleys that
551 developed lowered the water table and reduced seepage
552 flux rates to the point that sand could no longer be trans-
553 ported with available discharge.

554 4.2.2. Case 2: Shallow Effective Aquifer Depth ($h_e = 100$ m, $\beta = 0.00693$)

556 [32] A second simulation with the same material proper-
557 ties and recharge rate was conducted, but with the value of

β in equation (2) doubled relative to the previous simulation 558
such that the hydraulic conductivity decreased to half the 559
surface value at a depth of 100 m (Figure 1e). This has the 560
effect of decreasing the effective aquifer depth, h_e , in 561
equation (4), increasing hydraulic gradients, and increasing 562
the fraction of the land surface with seepage efflux (42% 563
initially, decreasing at the end of the simulation to about 564
19% as the eroded valleys lowered the water table and 565
captured most of the seepage). 566

[33] Under this set of conditions valley incision was 567
initiated at the base of a slope or crater wall and worked 568
its way headward but rarely reached close to the drainage 569
divides. The longitudinal profile of a valley pointed by 570
white arrow in Figure 1e clearly demonstrated this feature 571
(Figure 2). In comparison with the longitudinal profile 572
from solely fluvial erosion, the seepage erosion generated 573
valley is steeper at the head because of the headward 574
erosion. Valley deepening and extension occurred 575
throughout the simulation, producing low-gradient, wide, 576
stubby valleys with weak branching with an overall 577
pattern similar to that resulting from seepage weathering 578
in Figure 1f. In addition to the abrupt valley headwalls, a 579
diagnostic feature of seepage erosion of cratered land- 580
scapes is the scattered occurrence of nearly parallel flat- 581
floored drainages terminating at similar positions on 582
regional slopes, as in the locations marked with the 583
number sign in Figure 1e. 584

[34] Simulation runs with same parameters as above but 585
increasing sediment grain size to fine gravel result in no 586
channel development (not shown), which suggest that the 587
role of direct seepage erosion is probably limited on Mars. 588

589 4.3. Seepage Weathering of Bed Rock

[35] Under this scenario, groundwater seeps out to the 590
surface and causes accelerated weathering of the bedrock, 591
which is then more easily removed by fluvial processes. 592
This scenario targets the type of groundwater involvement 593
in canyon development in indurated sandstones, particularly 594
the Navajo Sandstone of the Colorado Plateau, USA. As 595
discussed earlier, values of hydraulic conductivity and 596
recharge rates are representative of the Navajo Sandstone 597
aquifer. Removal of seepage-weathered sediment is as- 598
sumed to occur by fluvial erosion dominated by discharge 599
from direct runoff. 600

601 4.3.1. Case 1: Strong Contribution of Seepage Weathering ($W_s = 0.002$)

[36] This simulation assumes a large seepage component 603
of weathering, W_s in equation (5) of 0.002. The concentrat- 604
ed weathering in zones of seepage results in the expected 605
morphology of sparse, weakly branched, deep canyons with 606
abrupt headwalls (e.g., the canyon to left of the number sign 607
in Figure 1f), although some background fluvial erosion 608
occurs without seepage involvement. The steep slope of 609
headwalls can also be seen in profile (Figure 2) of the valley 610
pointed by the white arrow in Figure 1f. The comparison 611
with the Colorado Plateau archetype assumes that the 612
seepage weathering, although in the natural setting involv- 613
ing weakening of a thin seepage face, undermines the 614
overlying rock (groundwater sapping), causing rockfalls 615
that pulverize much of the sandstone. Seepage may, in 616
addition, further weather the fallen debris [see, e.g., *Laity* 617
and Malin, 1985; *Howard and Kochel*, 1988]. In the 618

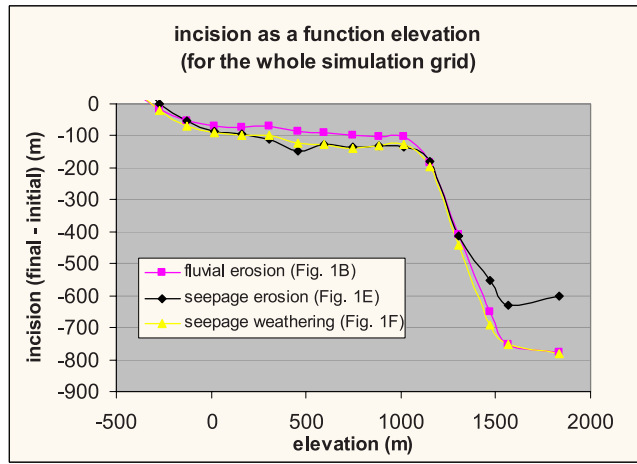


Figure 3. Distribution of incision as a function of elevation for Figures 1b, 1e, and 1f for the whole simulation grid. Incision is defined as final topography minus initial

619 Colorado Plateau setting removal of debris produced by
 620 seepage weathering is dominated by direct runoff from
 621 precipitation [Howard and Kochel, 1988; Lamb et al.,
 622 2006]. Discharge directly from seepage from sandstones
 623 with hydraulic conductivities and recharge rates character-

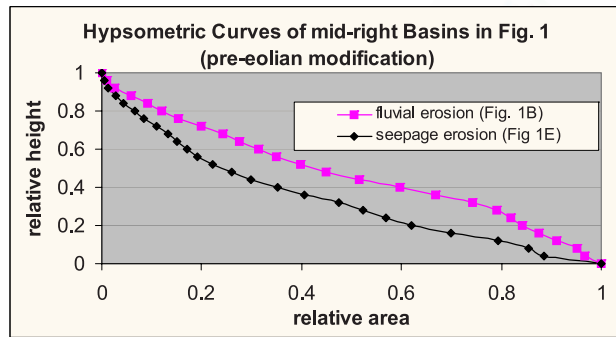
istic of the Navajo Sandstone is insufficient to transport
 even sand-size sediment [Lamb et al., 2006]. To confirm
 this, a simulation run (not shown) using the same param-
 eters as those in Figure 1f but with the surface water
 discharge being solely from groundwater seepage resulted
 in no fluvial erosion.

4.3.2. Case 2: Varying Relative Contribution of Seepage Weathering ($W_s = 0.001$)

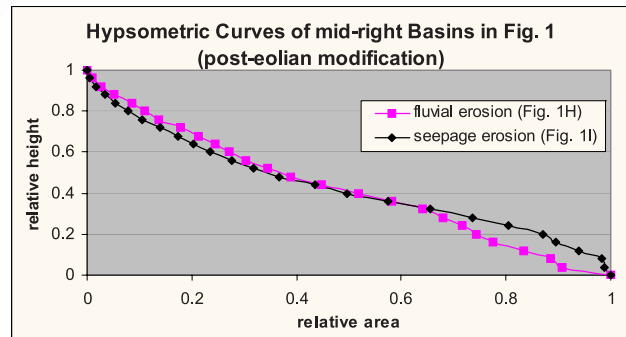
[37] A set of simulations were conducted with reduced
 values of the seepage weathering coefficient, W_s . One such
 simulation is shown in Figure 1g. As would be expected, the
 resulting pattern of fluvial incision was transitional between
 the strong seepage weathering in Case 1 (Figure 1f) and the
 solely runoff erosion case in Figure 1b. With a small W_s , the
 valleys are small and shallow, whereas a large W_s leads to
 bigger and deeper valleys that looks more like typical
 groundwater sapping valleys (compare the valley to left of
 the number sign in Figures 1f and 1g). So depending on the
 seepage weathering rate, different degree of dissection can
 be generated through seepage weathering.

4.4. Comparing Incision as a Function of Elevation

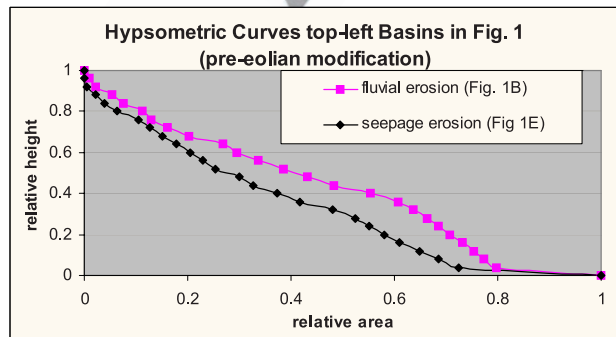
[38] To illustrate the channel incision as a function of
 elevation for different scenarios, we did the following
 calculation for fluvial erosion (Figure 1b), seepage erosion
 (Figure 1e), and seepage weathering (Figure 1f): (1) com-



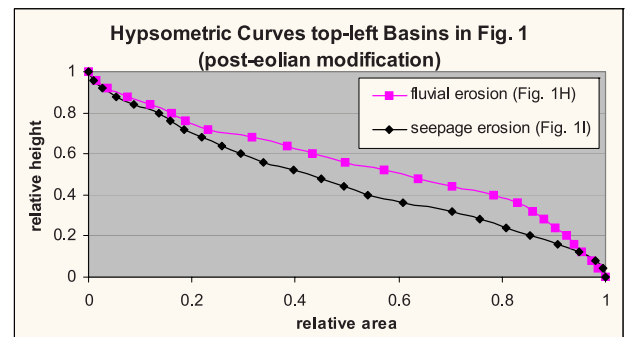
(A)



(B)



(C)



(D)

Figure 4. Hypsometric curve of the basin as outlined in Figures 1b, 1e, 1h, and 1i. Relative area is the area at a given elevation relative to the total area. Relative elevation is the elevation relative to the total relief of the basin. (a) Preeolian modification for the two midright basins. (b) Posteolian modification for the two midright basins. (c) Preeolian modification for the two top-left basins. (d) Posteolian modification for the two top-left basins.

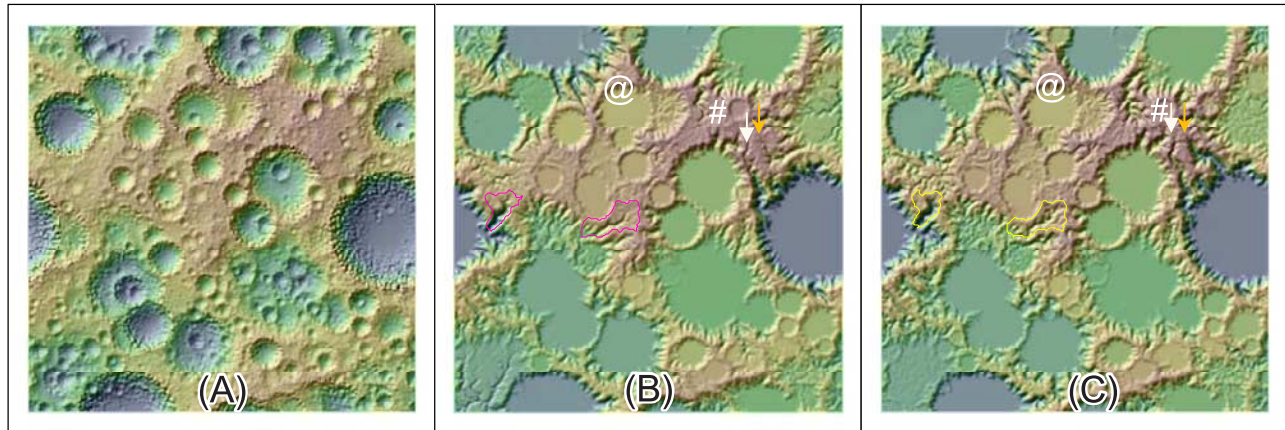


Figure 5. Simulation result from a different initial topographic condition. Color ramp from blue to brown indicates elevation from low to high. (a) initial topography, (b) fluvial erosion (using same parameter values as in Figure 1b), and (c) seepage weathering (using same parameter values as in Figure 1f).

649 pute the difference between the final topography and initial
 650 topography (negative values indicate incision); (2) divide
 651 the initial topography into 25 equal elevation zones; (3)
 652 calculated the average of the difference (or incision from
 653 calculation 1 within each zone (from calculation 2)); and (4)
 654 plot the average of incision in each zone as function of the
 655 zone elevation. The result is shown in Figure 3. For fluvial
 656 erosion there is smaller incision than seepage erosion and
 657 seepage weathering at lower elevation. At higher elevation,
 658 however, incision caused by fluvial erosion is similar to that
 659 by seepage weathering, because there is not much seepage
 660 at higher elevation anyway, and thus the erosion there is
 661 primarily due to regular fluvial erosion, which explains the
 662 similar incision there. For seepage erosion, again there is
 663 not much seepage at higher elevation, so the incision there
 664 is lower than the other two cases.

665 **4.5. Eolian Modification**

666 [39] In order to test the effect of eolian modification on
 667 valley network morphology, we used the end result of
 668 fluvial erosion (Figure 1b) and seepage erosion (Figure
 669 1e) as initial conditions and run eolian processes on them.
 670 The results are shown in Figures 1h and 1i. Comparing with
 671 Figures 1b and 1e, eolian processes smooth the landscape
 672 and make them look more similar. The sharply defined
 673 channels in Figures 1b and 1e are now shallower and more
 674 rounded. The short channels developed on the crater walls
 675 are also smoothed out. We also obtained the hypsometric
 676 curves of the basins outline in the figures (one located in the
 677 midright of the figure and the other top-left) and compared
 678 with their preeolian counterparts (Figure 4). In the preeolian
 679 situation, the difference primarily reflects the headward
 680 erosion, similar to the longitudinal profile shown in Figure
 681 2. However, eolian modification made these two curves
 682 more similar. This is especially the case for the midright
 683 basins (Figures 4a and 4b). The more difference for the top-
 684 left basins may be an artifact of the preeolian basins
 685 including parts of the flat area of the crater. In any case,
 686 this suggests that postformation modification may compli-
 687 cate the interpretation of the origin of valley networks.

688 **4.6. Different Initial Conditions**

[40] Simulation runs with different initial conditions
 689 resulted in generally similar landform patterns. One such
 690 example is shown in Figure 5. The total relief (difference of
 691 maximum and minimum elevations) of the initial topogra-
 692 phy (Figure 5a) is about 3.2 km, similar to that of Figure 1a
 693 (3.6 km). For the fluvial erosion result (Figure 5b) and
 694 seepage weathering result (Figure 5c), we used the exact
 695 same parameter values as the corresponding cases shown in
 696 Figures 1b and 1f (i.e., the only difference is the initial
 697 topography), respectively. In Figure 5b, we observe a
 698 typical fluvial channel west of the number sign draining
 699 north that starts small and increases downstream with
 700 increasing contributing area. In comparison, in the seepage
 701 weathering case shown Figure 5c, we see headward erosion
 702 created more stubby-looking channels surrounding the
 703 highland area marked by the number sign and steeper and
 704 bigger valley heads near “the at symbol” and in the basin
 705 near the west edge of the figure. It is interesting to note that
 706 headward erosion has caused the channel pointed by the
 707 orange arrow draining into the big crater (Figure 5c) to
 708

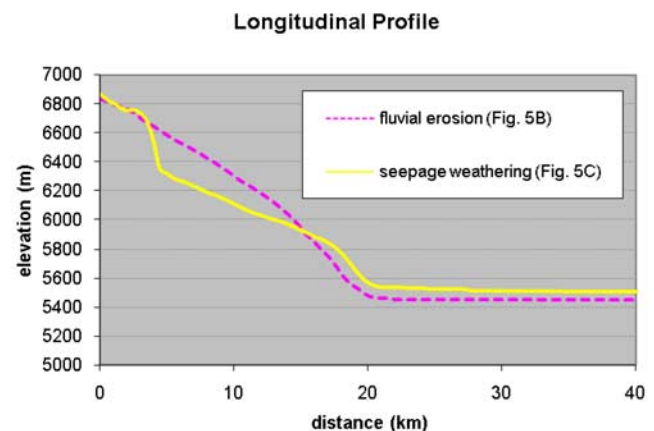
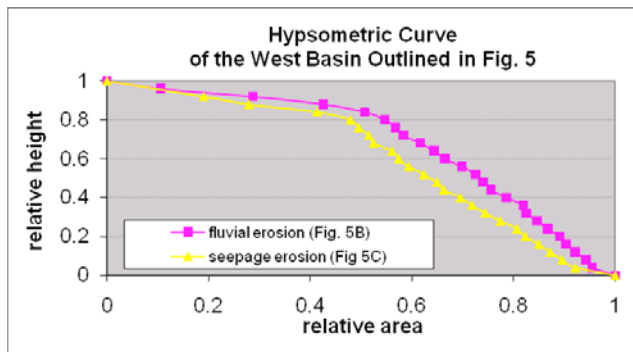
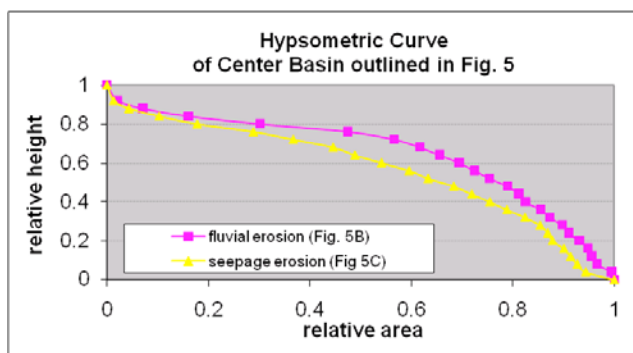


Figure 6. Longitudinal profile of channel pointed by the white arrow in Figures 5b and 5c.



(A)



(B)

Figure 7. Hypsometric curve of the basin outlined in Figure 5 (the (a) west basin and (b) center basin).

709 pirate another channel that was originally draining to the
 710 northeast shaped like the letter “L” (compare the channel
 711 pointed by orange arrow in Figure 5b). The effect of
 712 headward erosion can be seen more clearly in the longitudinal
 713 profiles of channels pointed by white arrows
 714 (Figure 6): at highest elevation, there is not much difference
 715 between seepage weathering and fluvial erosion, but be-
 716 tween about 5900 and 6600 m, headward erosion in seepage
 717 weathering caused more erosion and steeper slope than
 718 fluvial case. This general pattern is consistent with obser-
 719 vation made in Figures 2 and 3. The hypsometric curves of
 720 the outlined basins in Figure 5 are shown in Figure 7. These
 721 curves are similar to those in Figures 4a and 4c with
 722 seepage weathering having more overall erosion than the
 723 fluvial case. These hypsometric curves (Figures 4a, 4c, 7a,
 724 and 7b) all show more erosion for cases with groundwater
 725 involvement (seepage erosion or seepage weathering).
 726 However, the hypsometric curve of a typical groundwater
 727 sapping basin in Colorado Plateau is often seen less eroded
 728 than a typical fluvial basin [e.g., see Luo, 2000, Figure 4].
 729 We interpret this as being due to the initial cratered
 730 topography used in the simulation, as opposed to a nearly
 731 planar, sandstone-capped plateau as initial topography for
 732 the Colorado Plateau, which could allow more areas subject
 733 to groundwater seepage and thus causing more headward
 734 erosion. In summary, the overall simulation results and

morphometric attributes do not change with different initial 735
 condition. 736

5. Discussion 738

[41] We use a computer model to simulate the role of 739
 groundwater in forming Martian valley networks in two 740
 ways: (1) groundwater discharge contributes to surface 741
 water runoff, which causes additional erosion of unconsoli- 742
 dated sediments (seepage erosion) and (2) groundwater 743
 seepage causes accelerated weathering of bedrock, which 744
 makes its subsequent erosion and removal easier (seepage 745
 weathering). Simulations of both seepage weathering of 746
 indurated sediment and seepage erosion of fine cohesionless 747
 sediment produce valley networks that bear a distinctive 748
 morphology of being flat floored, weakly branched, low 749
 gradient, and ending in steep theater headwalls (e.g., Fig- 750
 ures 1e and 1f). This morphology has long been cited as 751
 being characteristic of groundwater involvement in valley 752
 network development, both in terrestrial settings [Laity and 753
 Malin, 1985; Kochel and Piper, 1986; Howard and Kochel, 754
 1988] and on Mars [Pieri, 1980a, 1980b; Higgins, 1982; 755
 Carr, 1995, 2002; Malin and Carr, 1999; Grant, 2000; 756
 Malin and Edgett, 2000; Grant and Parker, 2002]. The 757
 reason for the similarity between valleys produced 758
 by seepage erosion and those resulting from seepage 759
 weathering is that sediment transport is a positive function 760
 of groundwater-derived surface water flow rate, and, like- 761
 wise, we assume that seepage weathering is also a positive 762
 function of seepage efflux. 763

[42] A number of issues complicate using valley network 764
 morphology to infer process scenarios on Mars. The num- 765
 bered paragraphs below briefly summarize cautions in 766
 interpretation of valley network origin raised by Lamb *et* 767
al. [2006]. 768

[43] 1. Mass wasting, impact gardening [Hartmann *et al.*, 769
 2001], and eolian infilling of valleys (e.g., compare Figures 770
 1e and 1i) have so modified Martian valley networks that 771
 characteristic landforms such as seepage alcoves would not 772
 have survived to the present. Small headwater tributaries 773
 may have been destroyed, giving the appearance of low 774
 drainage densities and abrupt headward terminations of 775
 valley networks even if the drainage density were initially 776
 high and valleys extended close to divides. 777

[44] 2. Valleys with abrupt, theater-like headwalls might 778
 also be created by layered stratigraphy, such as erosion 779
 through indurated rocks (e.g., basalt flows) into underlying 780
 weak sediment (e.g., megaregolith, volcanic ash, or uncon- 781
 solidated sediment). Formation of duricrusts and subsequent 782
 erosion through the crusts are an additional possibility 783
 [Howard *et al.*, 2005]. 784

[45] 3. Fluvial erosion through layered stratigraphy fol- 785
 lowed by modification by mass wasting can produce the- 786
 ater-headed valley terminations [Howard, 1995; Lamb *et* 787
al., 2006]. 788

[46] 4. Some terrestrial theater-headed valley systems 789
 previously attributed to groundwater erosion, such as Ha- 790
 waiian valleys [Kochel and Piper, 1986] and box canyons 791
 eroded into lava flows in Idaho, may instead be formed by 792
 plunge pool erosion [Lamb *et al.*, 2006, 2007]. 793

[47] Although the present simulations of groundwater 794
 involvement in valley development produce characteristic 795

796 valley morphology that has long been attributed to seepage
797 processes, caution in interpretation should also be exercised
798 because of the restrictive material and process scenarios
799 necessary for appreciable groundwater contribution to ero-
800 sion. Direct erosion solely by groundwater seepage requires
801 subsurface materials with hydraulic conductivity at least
802 equal to that of cohesionless fine sand and high recharge
803 rates. Impact gardening might produce a megaregolith with
804 appropriate hydraulic conductivity [Clifford, 1993; Clifford
805 and Parker, 2001]. In addition, however, the presence of an
806 appreciable fraction of gravel or larger particles within the
807 substrate will produce a lag concentrate in valleys that
808 seepage discharges cannot transport. In such circumstances
809 erosion can continue only if weathering processes commi-
810 nute the large particles or if occasional direct runoff aids
811 removal of large particles. Such a process mix of seepage
812 undermining and runoff erosion is common in terrestrial
813 valley networks [e.g., Schumm and Phillips, 1986].

814 [48] Enhancement of valley incision by seepage weather-
815 ing also requires specific substrate properties and weather-
816 ing processes that may be restrictive. The subsurface aquifer
817 must be thick, relatively massive, and it must have appreci-
818 able hydraulic conductivity coupled with cementation
819 sufficient to sustain canyon walls while being susceptible
820 to seepage weathering processes. Aquicludes may help to
821 create seepage faces on valley walls. Even in the sandstones
822 of the Colorado Plateau this set of characteristics is rare, for
823 other thick sandstones, like the Wingate Formation and the
824 Coconino Sandstone rarely exhibit valleys with seepage
825 alcoves.

826 [49] Lamb *et al.* [2006] make the general observation that
827 processes involved in seepage weathering are uncertain
828 even for Earth, making extrapolation to Mars problematic.
829 If seepage weathering occurs primarily by freeze-thaw or by
830 crystal growth within seepage faces, then similar settings
831 may have occurred on early Mars. But if seepage weather-
832 ing on Earth is dominated by processes related to the nearly
833 universal covering of seepage faces by biotic crusts and
834 vegetation, then Martian counterparts are unlikely.

835 [50] Finally, the formation of valleys by groundwater
836 weathering requires concomitant episodic high-intensity
837 runoff from precipitation, either directly from rain or
838 through snowmelt, in order to transport the products of
839 seepage weathering from valley headwalls [Howard and
840 Kochel, 1988; Lamb *et al.*, 2006]. In the most widely cited
841 terrestrial example of valleys eroded into the Navajo Sand-
842 stone [e.g., Laitly and Malin, 1985], it is unclear to what
843 extent seepage weathering dominates valley extension as
844 compared to erosion in plunge pools and headwall under-
845 mining at the contact between the Navajo Sandstone and the
846 underlying Kayenta Formation [Lamb *et al.*, 2006].

847 [51] Although definitive identification of Martian fluvial
848 networks as having been influenced by seepage processes
849 may not be possible based upon remote sensing informa-
850 tion, some valley networks exhibit morphologies that both
851 resemble the simulated seepage-related valleys and which
852 have a topographic context that might have encouraged
853 groundwater involvement. One such setting is illustrated in
854 Figure 8a, where a high plateau on the east side of the image
855 lies about 1050 m above a northward-flowing drainage
856 (Marikh Valles) that enters at the number sign and exits to
857 the north at the at symbol. Several features of the tributary

858 valleys dissecting the edges of this plateau suggest seepage-
859 related erosion. Valleys eroded into the regional slope on the
860 north side of the plateau exhibit flat-floored morphology
861 and abrupt headwalls, e.g., the valleys in the top portion of
862 Figure 8c and the valleys northeast of “z.” Valleys eroded
863 into the west side of the plateau exhibit a parallel drainage
864 pattern with, again, abrupt terminations at a consistent
865 elevation about 100 m below the plateau surface, as in
866 Figures 8b and 8d and west of z. Both of these valley
867 morphologies are typical of fluvial incision by seepage
868 erosion or aided by seepage weathering (e.g., Figures 1e,
869 1f, and 5c). The broad, relatively undissected plateau
870 surface could have served as a recharge area for seepage
871 contributing to valley erosion. In Figure 8b a ledge near the
872 head of the valleys suggests the outcrop of a resistant layer
873 that could have encouraged seepage-related erosion by
874 having served either as an aquifer or an aquiclude.

875 [52] However, surface runoff must also have occurred
876 within the region shown in Figure 8. The crater at “x” has a
877 deeply eroded valley extending from an exit breach on the
878 southwest rim. The crater in Figure 8c also has an exit
879 breach through the south rim. The plateau surface also is
880 drained by a valley that has breached the divide at “y.”
881 These observations suggest that the valley networks may
882 have had a composite origin involving both seepage-related
883 erosion and surface runoff. The flat-floored valley heads in
884 the top portion of Figure 8 may have received seepage
885 discharge from standing water in the crater basin draining
886 underground beneath the crater rim.

887 [53] In summary, the valley system dissecting the plateau
888 in Figure 8 is consistent with joint involvement of surface
889 runoff with either seepage weathering or seepage erosion.
890 Alternatively, seepage processes might not have been im-
891 portant and the flat-floored valleys and parallel drainages
892 may simply reflect fluvial erosion into a layered stratigraphy
893 underlying the plateau.

6. Conclusions 894

895 [54] Our simulations have shown that erosion involving
896 seepage processes produces a distinctive morphology of
897 low-gradient flat-floored valleys with abrupt, theater-like
898 headwalls and weak branching. Such valleys generally do
899 not extend all the way to crater rims and major divides, and
900 seepage-related valleys cutting into regional slopes com-
901 monly exhibit a parallel drainage pattern with headwalls at a
902 consistent elevation on the regional slope. Seepage may be
903 involved in valley incision either through direct erosion if
904 the substrate is fine, cohesionless sediment or through
905 aiding weathering of indurated sediment.

906 [55] Under the first scenario, the fine cohesionless sedi-
907 ments could be generated by impact cratering and weather-
908 ing processes. However, groundwater seepage erosion could
909 not form any integrated valley networks for sediment
910 incorporating an appreciable fraction of gravel size or larger
911 sediment. Seepage erosion tends to cause more incision at
912 lower elevations. Erosion solely by runoff tends to cause
913 more incision at higher elevations. In the second scenario,
914 seepage weathering combined with fluvial runoff creates
915 stubby deep canyons with abrupt headwalls that are similar
916 in morphology to terrestrial and Martian valley systems
917 attributed to erosion by groundwater. At least occasional

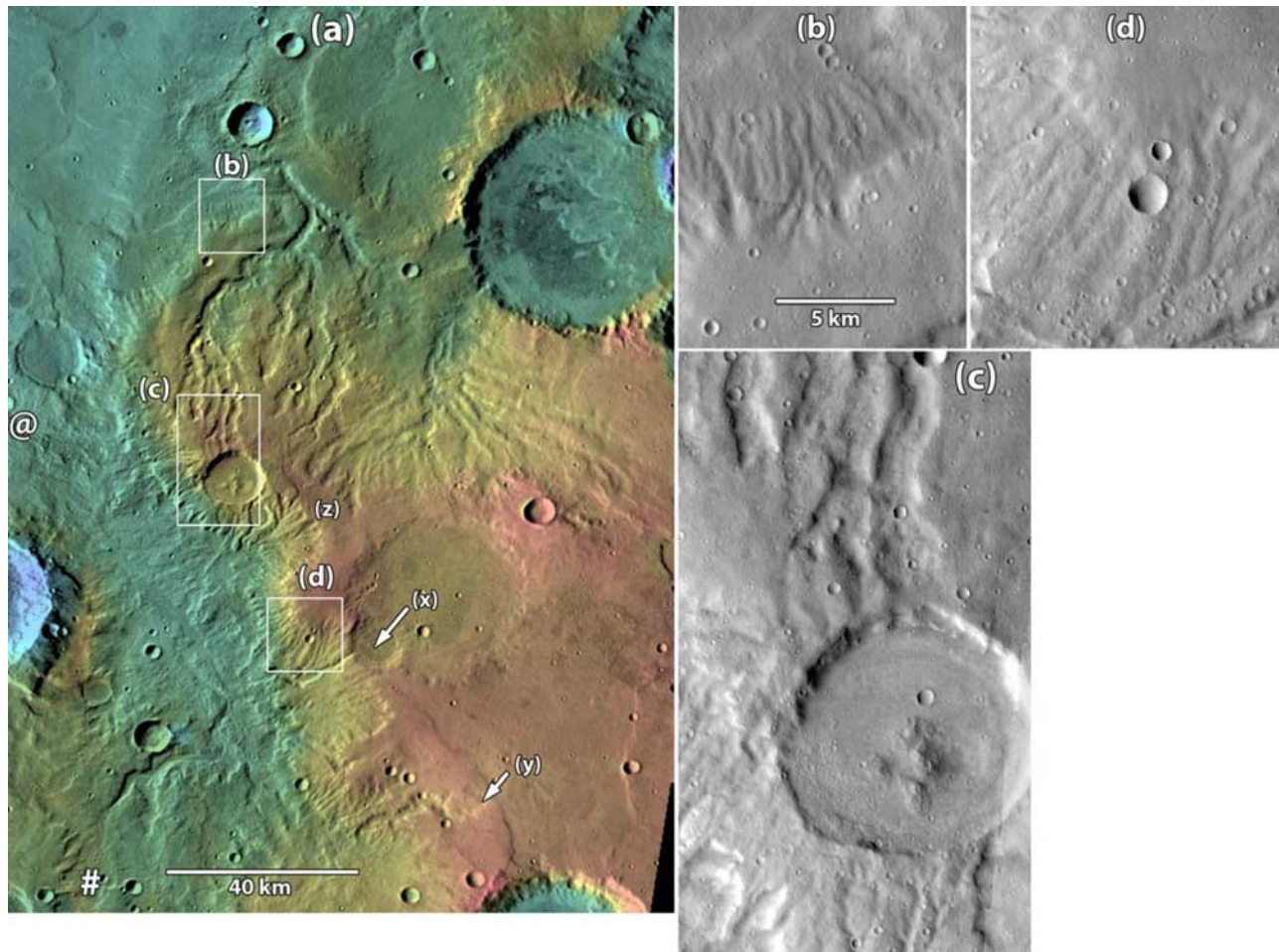


Figure 8. Martian plateau dissected by valleys possibly involving seepage-related erosion. (a) Thermal Emission Imaging System (THEMIS) daytime IR image mosaic with elevation color coding from Mars Orbiter Laser Altimeter PEDR topography. Image centered at about 5.8°E and 24.1°S. Boxes show location of insets. North is to top of image. (b) A portion of THEMIS visible light spectrometer (VIS) image V06317001. Scale applies to all insets. (c) A portion of VIS images V07428001 and V15615001. (d) A portion of VIS image V08152003. Images courtesy of Mars Space Flight Facility, Arizona State University at <http://themis-data.asu.edu> and Java Mission-Planning and Analysis for Remote Sensing at <http://jmars.asu.edu/data>.

918 direct runoff from precipitation is required to remove
 919 the weathering products of seepage weathering and mass-
 920 wasted debris produced by sapping of headwall cliffs. Thus
 921 we infer the role of groundwater in forming integrated
 922 Martian valley networks to be primarily through seepage
 923 weathering.

924 [56] Depending on seepage weathering rate, dissection of
 925 various degrees can be generated through seepage weather-
 926 ing. However, nonseepage related stratigraphic controls
 927 may produce valley morphology similar to that produced
 928 by seepage processes. In addition, postformation eolian
 929 modification may also make the landform resulted from
 930 sole surface runoff and that involving groundwater seepage
 931 similar both visually and from basin hypsometry, making
 932 interpretation difficult. Martian valley networks may have
 933 developed through a range of combinations of runoff
 934 erosion and seepage weathering, which can complicate the
 935 interpretation of the processes based on final landform
 936 morphology. Unequivocal identification of seepage involve-

ment of valley incision on Mars may not be possible 937
 without knowledge of subsurface properties (hydraulic 938
 conductivity, layering, degree of cementation, etc.) and the 939
 grain sizes of sediment transported through the valley 940
 systems. 941

[57] **Acknowledgments.** This research is funded by NASA Mars 942
 Data Analysis Program. 943

References 944

- Brown, J. G., and J. H. Eychaner (1988), Simulation of five ground-water 945
 withdrawal projections for the Black Mesa area, Navaho and Hopi Indian 946
 Reservations, Arizona, *U. S. Geol. Surv. Water Resour. Invest. Rep.*, 88- 947
 4000, 1-51. 948
 Budhu, M., and R. Gobin (1995), Seepage-induced slope failures on sand- 949
 bars in Grand Canyon, *J. Geotech. Eng.*, 121(8), 601-609, doi:10.1061/ 950
 (ASCE)0733-9410(1995)121:8(601). 951
 Carr, M. H. (1995), The Martian drainage system and the origin of valley 952
 networks and fretted channels, *J. Geophys. Res.*, 100, 7479-7507, 953
 doi:10.1029/95JE00260. 954
 Carr, M. H. (1996), *Water on Mars*, 229 pp., Oxford Univ. Press, New York. 955

- 956 Carr, M. H. (2002), Elevations of water-worn features on Mars: Implications for circulation of groundwater, *J. Geophys. Res.*, 107(E12), 5131, doi:10.1029/2002JE001845.
- 959 Clifford, S. M. (1993), A model for the hydrologic and climatic behavior of water on Mars, *J. Geophys. Res.*, 98(E6), 10,973–11,016, doi:10.1029/93JE00225.
- 962 Clifford, S., and T. Parker (2001), The evolution of the Martian hydro-sphere: Implications for the fate of a primordial ocean and the current state of the Northern Plains, *Icarus*, 154(1), 40–79, doi:10.1006/icar.2001.6671.
- 966 Coelho Netto, A. L. and N. F. Fernandes (1990), Hillslope erosion, sedimentation, and relief inversion in SE Brazil: Bananal, SP, in *Research Needs and Applications to Reduce Erosion and Sedimentation in Tropical Steeplands*, *Int. Assoc. Hydrol. Sci. Publ. Ser.*, vol. 192, edited by R. R. Ziemer et al., pp. 174–182, Int. Assoc. of Hydrol. Sci., Oxfordshire, U. K.
- 970 Craddock, R. A., and A. D. Howard (2002), The case for rainfall on a warm, wet early Mars, *J. Geophys. Res.*, 107(E11), 5111, doi:10.1029/2001JE001505.
- 974 Dunne, T. (1980), Formation and controls of channel networks, *Prog. Phys. Geogr.*, 4, 211–239, doi:10.1177/030913338000400204.
- 976 Dunne, T. (1990), Hydrology, mechanics, and geomorphic implications of erosion by subsurface flow, in *Groundwater Geomorphology: The Role of Subsurface Water in Earth-Surface Processes and Landforms*, edited by C. G. Higgins and D. R. Coates, pp. 1–28, *Geol. Soc. Am. Spec. Pap. Ser.*, vol. 252, Geol. Soc. of Am., Boulder, Colo..
- 981 Forsberg-Taylor, N. K., A. D. Howard, and R. A. Craddock (2004), Crater degradation in the Martian highlands: Morphometric analysis in the Sinus Sabaeus region and simulation modeling suggest fluvial processes, *J. Geophys. Res.*, 109, E05002, doi:10.1029/2004JE002242.
- 985 Freeze, R. A. and J. A. Cherry (1979), *Groundwater*, 604 pp., Prentice-Hall, Englewood Cliffs, N. J.
- 987 Froede, C. R., Jr., and E. L. Williams (2004), The origin, development, and eventual consolidation of the canyons comprising Providence Canyon State Park, Stewart County, Georgia, *Southeast. Geol.*, 43(1), 39–50.
- 990 Gabbard, D. S., C. Huang, L. D. Norton, and G. C. Steinhardt (1998), Landscape position, surface hydraulic gradients and erosion processes, *Earth Surf. Processes Landforms*, 23(1), 83–92, doi:10.1002/(SICI)1096-9837(199801)23:1<83::AID-ESP825>3.0.CO;2-Q.
- 994 Gehrels, W. R., and O. Van De Plassche (1992), Origin of the paleovalley system underlying Hammock River marsh, Clinton, Connecticut, *J. Coastal Res.*, 11, 73–83.
- 997 Gomez, B., and V. T. Mullen (1992), An experimental study of sapped drainage network development, *Earth Surf. Processes Landforms*, 17, 465–476, doi:10.1002/esp.3290170506.
- 1000 Grant, J. A. (2000), Valley formation in Margaritifer Sinus, Mars, by precipitation-recharged ground-water sapping, *Geology*, 28(3), 223–226, doi:10.1130/0091-7613(2000)28<223:VFJMSM>2.0.CO;2.
- 1003 Grant, J. A., and T. J. Parker (2002), Drainage evolution in the Margaritifer Sinus region, Mars, *J. Geophys. Res.*, 107(E9), 5066, doi:10.1029/2001JE001678.
- 1006 Gulick, V. C. (1998), Magmatic intrusions and a hydrothermal origin for fluvial valleys on Mars, *J. Geophys. Res.*, 103(E8), 19,365–19,387, doi:10.1029/98JE01321.
- 1009 Gulick, V., and V. R. Baker (1989), Fluvial valleys and Martian palaeoclimates, *Nature*, 341(6242), 514–516, doi:10.1038/341514a0.
- 1011 Gutierrez, B. T., E. Uchupi, N. W. Driscoll, and D. G. Aubrey (2003), Relative sea-level rise and the development of valley-fill and shallow-water sequences in Nantucket Sound, Massachusetts, *Mar. Geol.*, 193(3–4), 295–314, doi:10.1016/S0025-3227(02)00665-5.
- 1015 Hartmann, W. K., J. Anguita, M. A. de La Casa, D. C. Berman, and E. V. Ryan (2001), Martian cratering 7: The role of impact gardening, *Icarus*, 149, 37–53, doi:10.1006/icar.2000.6532.
- 1018 Heilweil, V. M., G. W. Freethey, C. D. Wilkowske, B. J. Stolp, and D. E. Wilberg (2000), Geohydrology and numerical simulation of ground-water flow in the central Virgin River basin of Iron and Washington Counties, Utah, *Tech. Publ. 116*, State of Utah Nat. Res., Salt Lake City.
- 1022 Heilweil, V. M., T. S. McKinney, M. S. Zhdanov, and D. E. Watt (2007), Controls on the variability of net infiltration into desert sandstone, *Water Resour. Res.*, 43, W07431, doi:10.1029/2006WR005113.
- 1025 Higgins, C. G. (1982), Drainage systems developed by sapping on Earth and Mars, *Geology*, 10(3), 147–152, doi:10.1130/0091-7613(1982)10<147:DSDBSO>2.0.CO;2.
- 1028 Higgins, C. G. (1984), Piping and sapping: Development of landforms by groundwater outflow, in *Groundwater as a Geomorphic Agent*, edited by R. G. Laffleur, pp. 18–58, Allen and Unwin, St Leonards, N.S.W., Australia.
- 1032 Howard, A. D. (1988), Groundwater sapping experiments and modeling, in *Sapping Features of the Colorado Plateau: A Comparative Planetary Geology Field Guide*, *NASA Spec. Publ. Ser.*, vol. 491, edited by A. D. Howard, R. C. Kochel, and H. E. Holt, pp. 71–83, NASA, Washington, D. C.
- 1035 Howard, A. D. (1994), A detachment-limited model of drainage basin evolution, *Water Resour. Res.*, 30(7), 2261–2286, doi:10.1029/94WR00757.
- 1038 Howard, A. D. (1995), Simulation modeling and statistical classification of escarpment planforms, *Geomorphology*, 12(3), 187–214, doi:10.1016/0169-555X(95)00004-O.
- 1040 Howard, A. D. (1997), Badland morphology and evolution: Interpretation using a simulation model, *Earth Surf. Processes Landforms*, 22(3), 211–227, doi:10.1002/(SICI)1096-9837(199703)22:3<211::AID-ESP749>3.0.CO;2-E.
- 1042 Howard, A. D. (2007), Simulating the development of Martian highland landscapes through the interaction of impact cratering, fluvial erosion, and variable hydrologic forcing, *Geomorphology*, 91, 332–363, doi:10.1016/j.geomorph.2007.04.017.
- 1047 Howard, A. D. and R. C. Kochel (1988), Introduction to cuesta landforms and sapping processes on the Colorado Plateau, in *Sapping Features of the Colorado Plateau: A Comparative Planetary Geology Field Guide*, *NASA Spec. Publ.*, vol. 491, edited by A. D. Howard, R. C. Kochel, and H. E. Holt, pp. 6–56, NASA, Washington, D. C.
- 1053 Howard, A. D., and C. F. McLane (1988), Erosion of cohesionless sediment by groundwater seepage, *Water Resour. Res.*, 24(10), 1659–1674, doi:10.1029/WR024i10p01659.
- 1057 Howard, A. D. and M. J. Selby (1994), Rockslopes, in *Geomorphology of Desert Environments*, edited by A. D. Abrahams and A. J. Parsons, pp. 123–172, Chapman and Hall, London.
- 1059 Howard, A. D., J. M. Moore, and R. P. Irwin III (2005), An intense terminal epoch of widespread fluvial activity on Mars: 1. Valley network incision and associated deposits, *J. Geophys. Res.*, 110, E12S14, doi:10.1029/2005JE002459.
- 1065 Irwin, R. P., III, A. D. Howard, and R. C. Craddock (2006), Theater-headed valleys: The roles of overland flow and groundwater sapping, *Lunar Planet. Sci. [CD-ROM]*, XXXVII, abstract 1912.
- 1066 Jones, J. A. A. (1971), Soil piping and stream channel initiation, *Water Resour. Res.*, 7, 602–610, doi:10.1029/WR007i003p00602.
- 1067 Jones, J. A. A. (1987), The effects of soil piping on contributing areas and erosion patterns, *Earth Surf. Processes Landforms*, 12(3), 229–248, doi:10.1002/esp.3290120303.
- 1070 Kochel, R. C., and J. F. Piper (1986), Morphology of large valleys on Hawaii: Evidence for groundwater sapping and comparison with Martian valleys, *J. Geophys. Res.*, 91, E175–E192, doi:10.1029/JB091iB13p0E175.
- 1074 Kochel, R. C., A. D. Howard, and C. McLane (1985), Channel networks developed by groundwater sapping in fine-grained sediments: Analogs to some Martian valleys, in *Models in Geomorphology*, edited by M. J. Woldenberg, pp. 313–341, Allen and Unwin, Winchester, Mass..
- 1077 Kochel, R. C., D. W. Simmons, and J. F. Piper (1988), Groundwater sapping experiments in weakly consolidated layered sediments: A qualitative summary, in *Sapping Features of the Colorado Plateau: A Comparative Planetary Geology Field Guide*, *NASA Spec. Publ.*, vol. 491, edited by A. D. Howard, R. C. Kochel, and H. E. Holt, pp. 84–93, NASA, Washington, D. C.
- 1082 Laity, J. E. (1983), Diagenetic controls on groundwater sapping and valley formation, Colorado Plateau, as revealed by optical and electron microscopy, *Phys. Geogr.*, 4(2), 103–125.
- 1086 Laity, J. E., and M. C. Malin (1985), Sapping processes and the development of theater-headed valley networks in the Colorado Plateau, *Geol. Soc. Am. Bull.*, 96, 203–217, doi:10.1130/0016-7606(1985)96<203:SPATDO>2.0.CO;2.
- 1089 Lamb, M. P., A. D. Howard, J. Johnson, K. X. Whipple, W. E. Dietrich, and J. T. Perron (2006), Can springs cut canyons into rock?, *J. Geophys. Res.*, 111(E7), E07002, doi:10.1029/2005JE002663.
- 1094 Lamb, M. P., A. D. Howard, W. E. Dietrich, and J. T. Perron (2007), Formation of amphitheater-headed valleys by waterfall erosion after large-scale slumping on Hawai'i, *Geol. Soc. Am. Bull.*, 119(7–8), 805–822, doi:10.1130/B25986.1.
- 1097 Lobkovsky, A. E., B. Jensen, A. Kudrolli, and D. H. Rothman (2004), Threshold phenomena in erosion driven by subsurface flow, *J. Geophys. Res.*, 109, F04010, doi:10.1029/2004JF000172.
- 1100 Luo, W. (2000), Quantifying groundwater sapping processes with a hypsometric analysis technique, *J. Geophys. Res.*, 105(E1), 1685–1694, doi:10.1029/1999JE001096.
- 1103 Luo, W., R. E. Arvidson, M. Sultan, R. Becker, M. K. Crombie, N. S. Sturchio, and Z. E. Alfy (1997), Ground-water sapping processes, Western Desert, Egypt, *Geol. Soc. Am. Bull.*, 109(1), 43–62, doi:10.1130/0016-7606(1997)109<0043:GWSPWD>2.3.CO;2.
- 1106 Malin, M. C., and M. H. Carr (1999), Groundwater formation of Martian Valleys, *Nature*, 397, 589–591, doi:10.1038/17551.
- 1107 Malin, M. C., and K. S. Edgett (2000), Evidence for recent groundwater seepage and surface runoff on Mars, *Science*, 288, 2330–2335, doi:10.1126/science.288.5475.2330.

- 1115 Mangold, N., and V. Ansan (2006), Detailed study of an hydrological
 1116 system of valleys, a delta and lakes in the Southwest Thamasia region,
 1117 Mars, *Icarus*, 180(1), 75–87, doi:10.1016/j.icarus.2005.08.017.
- 1118 Mangold, N., C. A. V. Quantin, and C. A. P. Delacourt (2004), Evidence for
 1119 precipitation on Mars from dendritic valleys in the Valles Marineris area,
 1120 *Science*, 305(5680), 78–81, doi:10.1126/science.1097549.
- 1121 Manning, C. E., and S. E. Ingebritsen (1999), Permeability of the conti-
 1122 nental crust: Implications of geothermal data and metamorphic systems,
 1123 *Rev. Geophys.*, 37(1), 127–150, doi:10.1029/1998RG900002.
- 1124 Montgomery, D. R., and W. E. Dietrich (1989), Source areas, drainage
 1125 density, and channel initiation, *Water Resour. Res.*, 25(8), 1907–1918,
 1126 doi:10.1029/WR025i008p01907.
- 1127 Nash, D. J. (1996), Groundwater sapping and valley development in the
 1128 Hackness Hills, North Yorkshire, England, *Earth Surf. Processes Land-
 1129 forms*, 21(9), 781–795, doi:10.1002/(SICI)1096-9837(199609)21:9
 1130 <781::AID-ESP616>3.0.CO;2-O.
- 1131 Ni, W. J., and H. Capart (2006), Groundwater drainage and recharge by
 1132 networks of irregular channels, *J. Geophys. Res.*, 111, F02014, doi:10.1029/
 1133 2005JF000410.
- 1134 Nwankwor, G. I., C. E. Dike, and C. J. Iwuagwu (1998), Piping, quick
 1135 conditions and liquefaction as factors of gully erosion: A case study of
 1136 Okwudor-Amucha gully complex, Imo State, Nigeria, *J. Min. Geol.*,
 1137 34(2), 225–230.
- 1138 Onda, Y. (2002), The effect of soil piping at seepage face on slope stability
 1139 and landform development, *Trans. Jpn. Geomorphol. Union*, 23(4),
 1140 647–658.
- 1141 Otvos, E. G. (1999), Rain-induced beach processes; landforms of ground
 1142 water sapping and surface runoff, *J. Coastal Res.*, 15(4), 1040–1054.
- 1143 Pieri, D. C. (1980a), Geomorphology of Martian valleys, in *Advances
 1144 in Planetary Geology, NASA Tech. Memo. 81979*, 1–362, NASA,
 1145 Washington, D. C.
- 1146 Pieri, D. C. (1980b), Martian valleys: Morphology, distribution, age, and
 1147 origin, *Science*, 210, 895–897, doi:10.1126/science.210.4472.895.
- 1148 Saar, M. O., and M. Manga (2004), Depth dependence of permeability in
 1149 the Oregon Cascades inferred from hydrogeologic, thermal, seismic, and
 1150 magmatic modeling constraints, *J. Geophys. Res.*, 109, B04204,
 1151 doi:10.1029/2003JB002855.
- 1152 Schumm, S. A. (1977), *The Fluvial System*, John Wiley, New York.
- Schumm, S. A., and L. Phillips (1986), Composite channels of the Canter- 1153
 bury Plain, New Zealand: A Martian analog?, *Geology*, 14(4), 326–329, 1154
 doi:10.1130/0091-7613(1986)14<326:CCOTCP>2.0.CO;2. 1155
- Schumm, S. A., K. F. Boyd, C. G. Wolff, and W. J. Spitz (1995), A ground- 1156
 water sapping landscape in the Florida panhandle, *Geomorphology*, 1157
 12(4), 281–297, doi:10.1016/0169-555X(95)00011-S. 1158
- Sharp, R. P., and M. C. Malin (1975), Channels on Mars, *Geol. Soc. Am.* 1159
Bull., 86(5), 593–609, doi:10.1130/0016-7606(1975)86<593:COM> 1160
 2.0.CO;2. 1161
- Shorghofer, N., B. Jensen, A. Kudrolli, and D. H. Rothman (2004), 1162
 Spontaneous channelization in permeable ground: Theory, experiment, 1163
 and observation, *J. Fluid Mech.*, 503, 357–374, doi:10.1017/ 1164
 S0022112004007931. 1165
- Spence, C. D., and D. J. Sauchyn (1999), Groundwater influence on valley- 1166
 head geomorphology, upper Battle Creek basin, Alberta and Saskatche- 1167
 wan, *Bull. Geol. Surv. Can.*, 534, 249–255. 1168
- Teixeira De Oliveira, M. A. (1990), Slope geometry and gully erosion devel- 1169
 opment: Bananal, Sao Paulo, Brazil, *Z. Geomorphol.*, 34(4), 423–434. 1170
- Thomas, B. E. (2002), Ground-water, surface-water, and water-chemistry 1171
 data, Black Mesa Area, northeastern Arizona–200–2001, and perfor- 1172
 mance and sensitivity of the 1988 USGS numerical model of the N 1173
 aquifer, *U. S. Geol. Surv. Water Resour. Invest. Rep.*, 2002–4211, 1–75. 1174
- Tomlinson, S. S., and Y. P. Vaid (2000), Seepage forces and confining 1175
 pressure effects on piping erosion, *Can. Geotech. J.*, 37(1), 1–13, 1176
 doi:10.1139/cgj-37-1-1. 1177
- Uchupi, E., and R. N. Oldale (1994), Spring sapping origin of the enigmatic 1178
 relict valleys of Cape Cod and Martha’s Vineyard and Nantucket Islands, 1179
 Massachusetts, *Geomorphology*, 9(2), 83–95, doi:10.1016/0169- 1180
 555X(94)90068-X. 1181
- Zhu, C. (2000), Estimate of recharge from radiocarbon dating of ground- 1182
 water and numerical flow and transport modeling, *Water Resour. Res.*, 1183
 36(9), 2607–2620, doi:10.1029/2000WR900172. 1184
-
- A. D. Howard, Department of Environmental Sciences, University of 1186
 Virginia, 291 McCormick Road, Charlottesville, VA 22903, USA. 1187
 (ah6p@virginia.edu) 1188
- W. Luo, Department of Geography, Northern Illinois University, Davis 1189
 Hall, Room 118, DeKalb, IL 60115, USA. (wluo@niu.edu) 1190